Pattern of shallow ground water flow at Mount Princeton Hot Springs, Colorado, using geoelectrical methods

K. Richards[1], A. Revil[1,2] , A. Jardani[1,3], F. Henderson[4], M. Batzle[1], and A. Haas[1]

(1) Colorado School of Mines, Dept of Geophysics, Golden, CO, USA

(2) LGIT, UMR C5559, Université de Savoie, 73376 Le Bourget-du-lac Cedex, France

(3) Université de Rouen, UMR 6143, CNRS, Morphodynamique Continentale et Côtière, Mt Saint Aignan, France

(4) Mount Princeton Geothermal Inc., Mount Princeton, CO, USA

Running title: Upflow of thermal water at a strike slip zone

Corresponding author: André Revil

Emails: ;

krichard@mymail.mines.edu; abderrahim.jardani@univ-rouen.fr

Intended for publication in Journal of Volcanology and Geothermal Research

Abstract. In geothermal fields, open faults and fractures often act as high permeability pathways bringing hydrothermal fluids to the surface from deep reservoirs. The Mount Princeton area, in south-central Colorado, is an area that has an active geothermal system related to faulting and is therefore a suitable natural laboratory to test geophysical methods. The Sawatch range-front normal fault bordering the half-graben of the Upper Arkansas valley is characterized by a right-lateral offset at Mount Princeton Hot springs. This offset is associated with the Chalk Cliffs of hydrothermally-altered quartz monzonite. Because fault identification in this area is complicated by quaternary deposits (including glacial and fluvial deposits), we use DC electrical resistivity tomography and self-potential mapping to identify preferential fluid flow pathways. The geophysical data (over 5600 resistivity and 2700 self-potential measurements) provide evidence of the existence of a dextral strike slip fault zone (Fault B) responsible for the offset of the Sawatch fault. A segment of this dextral strike slip fault (termed U1) is acting as the dominant vertical flow path bringing thermal waters to a shallow unconfined aquifer. Upwelling of the thermal waters is also observed at two zones (U2 and U3) of an open fracture called Fault A. This fault is located at the tip of the Sawatch fault and is likely associated with an extensional strain regime in this area. Self-potential measurements are used to estimate the flux of upwelling thermal water. The upflow estimate ($4\pm1 \times 10^3$ m^3/day for the open segment of the Fault B and $2\pm1 \times 10^3$ m^3/day for Fault A) from the geophysical data is remarkably consistent with the downstream Mt. Princeton hot water production ($4.3\text{-}4.9) \times 10^3$ m^3/day at approximately 60-65°C). A temperature map indicates that a third upwelling zone termed U4 may exist at the southern tip of the Sawatch fault.

1. Introduction

Faults play a major role in hydrogeology, acting as either high permeability conduits or barriers to groundwater flow, and in some instances can act as both (see Caine et al., 1996; Revil and Cathles, 2002; Fairley et al., 2003; Fairley and Hinds, 2004; Becken et al., 2008). This is especially relevant when considering the upwelling of thermal waters in most geothermal environments. Previous investigations have used geostatistical analyses of hot springs and ground temperatures to develop models for the distribution of permeability of faults in geothermal areas (e.g., Fairley et al., 2003; Fairley and Hinds, 2004; Heffner and Fairley, 2006). Recently, non-intrusive (geophysical) seismic and non-seismic (gravity, DC resistivity, self-potential, EM methods) methods have been shown to be useful for studying quantitatively ground water flow in geothermal areas (e.g., Aubert et al., 2000; Ishido 2004; Revil et al., 2008; Perrier et al., 2009; Legaz et al., 2009). In particular, the determination of the electrical resistivity distribution, from either DC resistivity tomography or EM methods and the self-potential method have been found to be complementary methods in characterizing hydrothermal systems (Garg et al., 2007; Jardani et al., 2008; Revil et al., 2008; Aizawa et al., 2009; Jardani and Revil, 2009).

The Mount Princeton hot springs area in the Arkansas Valley (Central Colorado) is a suitable field laboratory to test how geoelectrical methods can be used to constrain the pattern of ground water flow in the shallow (first 200 meters) subsurface. Mount Princeton is part of the Sawatch Range, which is oriented along a northwest-southeast axis on the western edge of the Upper Arkansas Valley. The Mount Princeton area represents a complex system where the interaction of faults has resulted in a series of hot springs including the Hortense Hot Spring, which is the hottest spring in Colorado (Limbach, 1975). However, fault identification is complicated by quaternary deposits including glacial deposits. This is why geophysical

methods are very useful in this context to locate faults and preferential ground water pathways associated with faulting.

In the present work, we performed 12 DC-resistivity profiles (1.26 km each) and over 2700 self-potential measurements to evidence and characterize the position of faults and the pattern of shallow ground water flow. We are especially interested to explore the potential role of a Precambrian strike slip transfer fault segmenting the Sawatch normal fault as a conduit for the upflow of thermal water. In addition to resistivity data, we used self-potential data to assess where the upwelling of hydrothermal water is taking place along the dextral strike slip fault zone and to quantify the flux of water over the area.

2. Geological and Geochemical Background

The Upper Arkansas Valley is a half-graben located between the Sawatch Range to the west and the Mosquito Range to the East with the main fault (the so-called Sawatch Range Fault) located to the west in the Arkansas Valley. This normal fault is characterized by northwest trending bordering the Sawatch Range. The Swatch Range, to the west of the Sawatch Fault, is composed by the (34-38 Ma) granitic batholith of Mt. Aetna volcanic volcano that was uplifted during the formation of the rift (Figure 1). To the east of the Sawatch Fault, sediments overlay the basement rocks at a depth of 2 km (Blum et al., 2009). These sediments are characterized by Miocene and Pliocene fluvial silts, sands, and gravels, referred to as the Dry Union Formation. In turn, these deposits are overlain by glacial, fluvial and alluvial deposits.

Normal faults such as the Sawatch Range fault can be segmented by transfer faults or accommodation zones (Gibbs, 1984; Bruhn et al., 1987; Miller 1999; McCalpin and Shannon, 2005). These boundaries can be described as conservative or non-conservative, depending on the slip vector relationship between the two segments of the main fault. A non-conservative

boundary results in a new direction of faulting in order to transfer motion between the two fault segments. The character of the southern face of Mount Princeton provides evidence of a non-conservative geometric segment boundary characterized by an east-west trending normal fault and related fracture system (Figures 1 and 2). The surface expression of this segmentation corresponds to the Chalk Cliffs, named for the white color of the highly fractured and hydrothermally altered quartz monzonite (Figures 2c). The main mineral resulting from alteration is kaolinite (replacing feldspar). This clay is characterized by a low cation exchange capacity and therefore a relatively low electrical surface conductivity by comparison with illite and smectite (Revil et al., 1998). The fracturing and alteration of the Chalk Cliffs makes also this zone subject to strong debris flows (Coe et al., 2008).

The history and sequence of this alteration/mineralization of Chalk Cliff has been studied in detail by Miller (1999). Miller (1999) suggested a breaching model to explain the segmentation of the Sawatch Range fault at Chalk Cliffs (Figure 2a). Similar models have been proposed for similar fault segmentation in extensional systems. Faulds and Varga (1998) for instance suggested that offset fault segments can be accommodated by a series of ramp-fault structures in an accommodation zone with no actual shear offset and strain within the rigid fault blocks.

However, this viewpoint is challenged by another interpretation. Some researchers have interpreted the northern and southern segments of Sawatch Range fault as being offset, at Chalk Cliffs, by a Precambrian transfer fault. This fault, shown with a northeast-southwest trend, may correspond presently to a dextral strike slip fault (Figure 2b) but there is no direct evidence that is has a strike-slip motion. We name this fault "Fault B" below. This fault would have been periodically stressed and reactivated over its history and would have moved in one direction or the other depending on the tectonic stresses. This transfer zone would have served as a boundary between the southern and northern sections of the Mount Aetna caldera

collapse (34 Ma) (Frederic Bergman, personal communication, 2010). The last activity of this transfer fault would have been contemporaneous of the activity of the rift system of the Arkansas valley (10-12 Ma).

Limbach (1975) indicated that evidences of such a transfer fault are found in the thermal alteration pattern, the non-alignment of the mountain front at Chalk Creek (South of chalk creek, the base of Mount Antero is offset about 2 km west, Figure 2c), and the linear character of the Chalk Creek valley (see also Crompton, 1976, and Arestad 1977). As shown below, our geophysical data further support the idea of a dextral strike slip fault zone explaining the offset of the Sawatch Range fault in the Chalk Creek area.

Dimick (2007) performed an extensive work regarding the composition of the thermal and non-thermal waters in the Mount Princeton area (see Table 1 and 2, respectively). Because of the very small amount of dissolved salts, the thermal water has a quite low electrical conductivity. Its origin is from the snowmelt of Mount Princeton infiltrating the ground in fractured areas not necessarily on Mount Princeton itself. Tritium analysis at Hortense Hot Springs shows that the residence time of this water is roughly 20-50 years inside the plumbing system of the hydrothermal system (Olson and Dellechaie, 1976). Assuming that there is no heat loss during the ascent of the thermal waters, the temperature of the thermal reservoir at depth is in excess of 150°C (Morgan and Sares, 2009). This result is consistent with estimates of the reservoir temperature from ionic geothermometers (Na-K; Na-K-Ca) (Morgan and Sares, 2009). Pearl (1979) estimated the subsurface geothermal reservoir temperatures for Mt. Princeton Hot Springs at 182 ºC and Coe (1978) used a reservoir temperature of 200°C.

3. Geophysical Investigations

3.1. Motivation

Self-potential is a passive electrical potential measurement of the electrical field that is created by the current associated with the flow of the groundwater within permeable earth materials. Indeed, the pore water of natural porous rocks carries usually an excess of electrical charge to counterbalance the charge deficiency of the mineral surface of silicates and aluminosilicates (see modeling in Revil and Leroy, 2001; Hase et al., 2003; Leroy and Revil 2004, Aizawa, 2008 and references therein). The drag of this excess of charge by the flow of the pore water creates an electrical current called the streaming current and, in turn, this current is responsible for electromagnetic disturbances that can be described by the low-frequency limit of the Maxwell equations (Malama et al., 2009a, b). The quasi-static electrical field produced at the ground surface of the Earth can be measured with a pair of non-polarizing electrodes and a high impedance calibrated voltmeter. It is called the self-potential field.

The combination of self-potential and DC resistivity data can be used to locate areas of upwelling water flow in geothermal systems along cracks and faults as shown by Ishido (2004), Jardani et al. (2008), and Jardani and Revil (2009), for instance. Ishido (2004) showed that self-potential signals, measured at the ground surface of the Earth, can be strongly influenced by the distribution of the DC resistivity of the subsurface and therefore requires DC resistivity to be properly modeled. The data collected in a resistivity survey can be used to create an image of the subsurface and it is a classical method of locating important subsurface features like faults (see Suski et al., 2010; Gélis et al., 2010 for recent examples). However, despite the fact that resistivity is sensitive to porosity, pore fluid composition, and temperature, there is not necessarily a correspondence between resistivity and permeability or lithology. Therefore, DC resistivity and self-potential cannot be used as stand-alone methods to infer permeable pathways. However, if combined, they offer a powerful approach to detect

and quantify ground water flow paths.

A number of recent studies have applied the self-potential and resistivity methods to solving groundwater flow problems (Byrdina et al., 2009; Jardani et al., 2009; Onizawa et al., 2009 for recent references). Researchers have successfully applied the self-potential method to ascertain the permeability distribution and anisotropy of aquifers and to invert the shape of the water table in steady-state conditions (see Wishart et al., 2006, Straface et al., 2007, and Jardani et al., 2009, for instance). Several studies have applied the self-potential method to qualitatively describe the pattern of subsurface water flow associated with volcanoes and geothermal systems (see Ishido, 1989, 2004; Ishido and Pritchett, 1999; Revil et al., 2001; Aizawa, 2004; Bedrosian et al. 2007) including the detection of faults acting as preferential fluid flow pathways (e.g., Revil et al., 1998). The research presented by Jardani et al. (2008) demonstrates how resistivity data and the relationship between self-potential data and the Darcy velocity can be used to quantitatively identify the position of transmissive fracture and to retrieve the associated flux of water (see also Onizawa et al., 2009). This approach will be used below to assess an order of magnitude of the flux of the thermal waters at Mount Princeton Hot Springs area.

3.2. Description of the Geophysical Surveys

Data collection consisted of a series of geophysical surveys performed in May 2008, September 2008, May 2009, and May 2010. The surveys resulted in over 2700 self-potential measurements (see Figures 3 and 4) and 12 long (~1.26 kilometers) resistivity profiles termed P1 to P12 below (see position on Figure 5). Some representative self-potential and resistivity tomograms are shown in Figure 6 to 10.

The self-potential measurements were performed with $Pb/PbCl_2$ non-polarizing electrodes from Geonesis and a high impedance Metrix voltmeter with an internal impedance

of 100 Mohm and a sensitivity of 0.1 mV. Measurements were repeatable to within 5 mV on average.

The resistivity data were obtained with an ABEM SAS-4000 resistivity meter using mainly the Wenner-α arrays and 64 stainless steel electrodes with a 20 m take-out unless otherwise specified. Salty water was added to the ground to decrease the contact resistance between the electrodes and the ground when needed. Most of the time, a current of 200 mA was injected in the ground. Each measurement was repeated until the standard deviation was below 5% (a maximum of 16 measurements were stacked together). Each profile was realized with a set of 64 stainless steel electrodes and comprises a total of 472 measurements.

Resistivity data were inverted with the commercial software RES2DINV (Loke and Barker, 1996) using a Gauss-Newton method and a finite element solver. The 2D assumption underlying the resistivity profiles implies that we tried to setup the profiles perpendicular to the structural heterogeneities. The mean RMS errors in the inverted resistivity profiles were generally below 10% except for profile P4 for which it reached 38%. The high RMS error on profile P4 is explained by the high resistivity of the quartz monzonite on the upper section of this profile that is much less altered by comparison with other profiles. Therefore it was difficult to inject a current higher than 50 mA in this portion of this profile.

Temperature was also recorded along Profile P3 using the same approach as reported by Revil et al. (2008) and references therein. Temperature measurements were made at a depth of 30±5 cm and were measured at equilibrium.

4. Interpretation of the Geophysical Data

We first propose a simplified qualitative interpretation of the characteristic resistivity and self-potential profiles shown in Figures 6 to 10. In Figure 11, we describe 6 types of typical self-potential anomalies encountered in geothermal systems. Type I corresponds to

positive anomalies associated with areas of upwelling of the ground water (Poldini, 1938; Ishido and Pritchett, 1999; Ishido, 2004; Byrdina et al., 2009). Type II corresponds at the opposite to negative anomalies associated with areas of ground water recharge (Poldini, 1938). Type III corresponds to the classical self-potential anomaly associated with ground water flow in an unconfined aquifer (Ishido and Pritchett, 1999; Revil et al., 2003, 2008). Type IV would be observed in absence of flow or of the flow is perpendicular to the self-potential profiles. Type V corresponds to the horizontal flow along an area of high hydraulic transmissivity (see Revil et al., 2005). Type VI corresponds to the vertical flow in the vadose zone as shown by Aubert et al. (2000) for instance.

4.1. Role of Fault B

The strike slip fault B is crossed and identified by several profiles (P1, P2, P3, P4, P6, and P8, see Figure 5). The combined data from the self-potential measurements and the resistivity profiles provide two complementary lines of evidence regarding the existence of this dextral strike slip fault zone. For instance, DC Resistivity tomograms on Profiles P4 and P3 show the fault as a ~150 m wide, near-vertical low-resistivity anomaly. This low resistivity anomaly corresponds to the fault damage zone, possibly associated with hydrothermal alteration and the flow of 60° thermal water. Resistivity anomalies B2, B3, and B4 shown in Figures 6 through 8 are aligned in a direction that is consistent with the presence of a dextral strike slip fault B (see position on Figures 2 and 3). Figure 3 shows clearly a drop in the self-potential signals associated with the presence of Fault B.

Additionally, Profile P3 (Figure 7) shows a clear positive self-potential anomaly associated with the conductive anomalies B3. We interpret this positive anomaly as being due to the upwelling of thermal waters along this portion of the dextral strike slip fault zone (self-potential anomaly of Type I). This self-potential anomaly is followed, further downslope, by a self-potential anomaly of Type III. Therefore, we interpret this sequence of anomalies has

been due to the upflow of thermal water along a segment of Fault B (acting as an open conduit) followed by the flow of the thermal water in an unconfined aquifer. The positive self-potential anomaly is also associated with a thermal anomaly (see the upper section of Figure 7).

At the opposite, Profile P4 does not exhibit such a clear positive anomaly. This would indicate that the dextral strike slip fault zone starts to be sealed at the position of Profile P4, a conclusion reinforced by the fact that there is no self-potential anomaly further south (see Figure 3). The same situation arises further north past the junction between the Northern segment of the Sawatch Fault and Fault B. In conclusion only a portion of Fault B represents a permeable pathway for the upwelling of the thermal water. This segment is in the vicinity of the tip of the northern segment of the Sawatch fault.

4.2. Role of Fault A

The electrical resistivity pattern exhibited by profiles P1 and P2 as well as their self potential anomalies are more complex. Figure 8 shows a positive self-potential anomaly (~70 mV, see Figure 4) is located in the hanging wall of Fault B at the tip of the Sawatch normal fault. This area corresponds probably to an extensional strain regime favoring the formation of tensile cracks acting as preferential conduits for the upwelling of the thermal waters. This upwelling is evidenced by two positive self-potential anomalies (type I) shown in Figure 4 along a conduit that we call Fault A. We term these two self-potential anomalies corresponding to upwelling zones U2 and U3. The fault A may be just a tensile crack not yet plugged by silica precipitation and channeling the thermal water from the deep reservoir to the shallow aquifer associated with Chalk Creek.

4.3. Role of The Sawatch Fault and Fault C

The Sawatch fault is intercepted by Profile P7 (see Figures 5 and 9). This profile does not exhibit any Type I (positive) self-potential anomaly. This means that there is no upwelling of thermal water on this segment of the Sawatch fault. We cannot demonstrate that this is however the case all along this fault. We only see a negative anomaly (maybe Type V) further East from the Sawatch fault indicating a preferential fluid flow pathway channeling the cold water along the fault further south, in agreement with the cold waters observed in the domestic wells in this area.

In the south part of the investigated area, Profiles P9 and P10 (Figure 10) show the presence of an additional fault that we named Fault C. This flow is in the direction of the flow in a shallow aquifer as shown in Section 5 from the piezometric data. This feature explains the absence of strong self-potential anomalies along Profiles P9 and P10 at the position of this fault. The position of this can be seen also on the self-potential anomaly of Profile P3 (at the bottom of the profile). Because of the change in self-potential trends in Profiles 3 and 6 at the fault position, this fault could act as a permeability barrier. Therefore the thermal waters channeled in the shallow aquifer below Chalk cliff could change direction and may follow this fault along the Chalk Creek River at the bottom of the valley.

5. Pattern of Ground Water Flow

While the previous section was qualitative, we try here to get a rough order of magnitude of the upflow of the thermal water along Faults A and B and get the picture of ground water flow at Mount Princeton Hot Springs. We first want to determine the flux of water coming from the open portion of Fault B. Revil et al. (2010) developed a self-potential tomography algorithm (based on the Gauss-Newton method) to determine the Darcy velocity (flux of water) along a tectonic fault. They applied their methodology to Profile P3 dividing the hydrogeological system into three units. The unit Un1 corresponds to the fault, Un2 to the

granitic basement, and Un3 to the shallow aquifer (see Figure 12). The presence of this shallow aquifer is confirmed by the drill-hole MPG-5 in the vicinity of the bottom of Profile P3. Hot water (59°C) was found in the MPG-5 well. The water table was located at a depth of 40 m and the depth of the well reaches 47 m.

The result of the inversion performed by Revil et al. (2010) is shown in Figure 12 (at the 61st iteration using a Gauss-Newton algorithm) and a comparison of the fit between the measured self-potential data and those associated with the optimized ground water flow model is shown in the insert of Figure 12 (RMS Error=1.2%). Their approach results in a mean Darcy-velocity of $7\pm2 \times 10^{-7}$ m s^{-1} in the fault plane (upflow area U1). Taking a fault thickness of 150 m as suggested from the resistivity tomograms and an open segment to fluid upflow of ~500 m along Fault B, a rough estimate of the flux of water is $4\pm1 \times 10^3$ m^3/day of thermal water upwelling along the fault plane at Chalk Cliff at a temperature of roughly 85°C. A similar approach applied to the two main positive anomalies shown along Fault A (Figure 4) yields an estimate of $2\pm1 \times 10^3$ m^3/day.

The previous upflow estimate (a total of $6\pm1 \times 10^3$ m^3/day) can be compared with the Mt. Princeton hot water production, which is about $(4.3\text{-}4.9) \times 10^3$ m^3/day at ~60-65°C. This production does not account for the presence of six fractures leaking directly into Chalk Creek below the pool to the west end of Mount Princeton Hot Springs property.

The compilation of all the geophysical data (resistivity and self-potential) plus the piezometric levels is shown in Figure 13. Figure 13 shows the source of thermal water associated with the Faults A and B and the direction of ground water flow perpendicular to the hydraulic equipotentials. The red arrows correspond to the flow of the direction of the flow of the thermal water and the blue arrows underline the flow of the cold water. We have also shown the position of the wells (hot, warm, and cold). There is a great consistency between this flow model and the position of the hot and cold domestic wells shown in Figure 13.

Figure 14 shows temperature data measured or extrapolated at a depth range comprised between 20 to 50 m. Possible sources for the cold waters come from the foothills of Mount Princeton and Mount Antero bordering Chalk Creek. The position of the thermal water upflow areas (U1, U2, and U3 associated with the Faults A and B, see Figures 13 and 14) explain vey well the temperature distribution in the north part of the investigated area. However, there is the need to invoke an additional upwelling zone further south (that we termed U4, see Figure 14) to explain the high temperatures (40-60°C) along the Western part of Fault C. The drillhole MPG-1 (see position in Figure 5) intersected a fractured aquifer in the quartz monzonite with a temperature of ~67°C at a depth of 149 m. This fractured quartz monzonite aquifer carrying hot water is also recognized in several domestic drillholes in this area. This thermal water may come with an upwelling area U4 located at the tip of one of the southern segments of the Sawatch fault as there are no positive self-potential anomalies in the investigated area including at Dead Horse Lake (see Figure 3).

6. Conclusions

This research provides significant evidence that supports the existence of a dextral strike slip fault zone (Fault B) as potentially responsible for the offset in the Sawatch Range normal Fault in the Mount Princeton area. This is seen in the complementary anomalies shown in both the DC resistivity and self-potential surveys. A portion of this dextral strike slip fault zone (area U1) and the presence of an open fracture at the tip of the Sawatch fault (Fault A with upwelling areas U2 and U3) act both as high permeability flow conduits, resulting in the expression of hot water (60-65°C) near the ground surface from a deep hydrothermal reservoir with a temperature at 150°C. The flow along the fault is possibly driven primarily by buoyancy.

This research also demonstrates the benefits of applying DC resistivity and self-potential to the characterization of hydrothermal systems. These methods provide two lines of evidence that show the position of the fault and provide a quantitative estimate of the flux of the upwelling water, especially important when considering a source for geothermal energy development. It would be interesting to see how the present model applies to two other transfer zones along the Arkansas valley known to be the setting of observable hydrothermal activity: to the north at the site of Cottonwood and Charlotte Hot Springs and in the south at the site of Poncha Hot Springs. Self-potential could be also used to detect geothermal systems along the Upper Arkansas valley that may exist without surface manifestations. Additionally, such geophysical data are useful for the development of a reactive flow transport model to further understand the plumbing system when combined with other types of data such like pore water mineral composition and temperature. Such modeling will not only aid in geothermal energy development, but can provide additional knowledge in understanding the precipitation/dissolution reactions of the fracture system and improve understanding of the evolution of the tectonic behaviors of rift systems in general.

Acknowledgements. We thank the DOE (Energy Efficiency and Renewable Energy, Geothermal Technologies Program), Award GO18195 "Use of Geophysical techniques to characterize fluid flow in a geothermal reservoir", for funding. We thank the students of the 2008 and 2009 GP field sessions and especially J. Buczyns, B. Hart, J. Havens, and S. Pathira. We thank Fred Berkman and R.G. (Bob) Raynolds for their advices in the field and all the private owners of the Mount Princeton area for access to their properties (especially Bill Moore). We thank the SEG Foundation, CGG Veritas and Sercel, and Chaffee County for their supports, Dear Valley Ranch for providing the lodging, and the local community for their support.

References

Aizawa, K., 2004. A large self-potential anomaly and its changes on the quiet Mount Fuji, Japan. Geophys. Res. Lett. 31, L05612, doi:10.1029/2004GL019462.

Aizawa, K. 2008, Classification of self-potential anomalies on volcanoes and possible interpretations for their subsurface structure. J. Volcanol. Geotherm. Res. 175, 253-268, doi:10.1016/j.jvolgeores.2008.03.011.

Aizawa, K., Ogawa, Y., Ishido, T., 2009. Ground water flow and hydrothermal systems within volcanic edifices: delineation by electric self-potential and magnetotellurics. J. Geophys. Res. 114, B01208, doi: 10.1029/2008JB005910.

Arestad, J.F., 1977. Resistivity studies in the upper Arkansas Valley and northern San Luis Valley, Colorado. MS thesis, Colorado School of Mines.

Aubert M., Dana, I. N., Gourgaud, I. A., 2000. Internal structure of Merapi summit from self-potential measurement. J. Volcanol. Geotherm. Res. 100, 337-343.

Becken, M., Ritter, O., Park, S. K., Bedrosian, P. A., Weckmann, U., Weber M., 2008. A deep crustal fluid channel into the San Andreas Fault system near Parkfield, California. Geophy, J. Int. 173, 718-732.

Blum T., van Wijk, K., Liberty, L., Batzle, M., Krahenbuhl, R., Revil, A., 2009. Characterization of a geothermal system in the Upper Arkansas Valley, Colorado, SEG Meeting, Session MIN P1 "Case Histories and Technology", Wednesday, October 2009, Houston, TX.

Bolève, A., Crespy, A., Revil, A., Janod, F., Mattiuzzo, J. L., 2007. Streaming potentials of granular media: Influence of the Dukhin and Reynolds numbers. J. Geophys. Res. 112, B08204, doi:10.1029/2006JB004673.

Byrdina, S., Revil, A., Pant, S. R., Koirala, B. P., Shrestha, P. L., Tiwari, D. R., Gautam, U.

P., Shrestha, K., Sapkota, S. N., Contraires, S., Perrier, F., 2009. Dipolar self-potential anomaly associated with carbon dioxide and radon flux at Syabru-Bensi hot springs in central Nepal. J. Geophys. Res. 114, B10101, doi:10.1029/2008JB006154.

Caine, J.S., Evans, J.P., Forester, C.B., 1996. Fault zone architecture and permeability structure. Geology 24, 1025 – 1028.

Coe, B. 1978. Geothermal Energy Development in Colorado: Processes, Promises and Problems. Colorado Geological Survey, Information Series 9, pp. 1-48.

Coe, J.A., Kinner, D. A., Godt, J. W., 2008. Initiation conditions for debris flows generated by runoff at Chalk Cliffs, Central Colorado. Geomorphology 96, 270–297.

Colman, S.M., McCalpin, J.P., Ostenaa, D.A., Kirkham, R.M., 1985. Map showing upper Cenozoic rocks and deposits and Quaternary faults, Rio Grande Rift, south-central Colorado. U.S. Geological Survey Miscellaneous Investigations Map I-1594, scale 1:125,000.

Crompton, J.S., 1976. An active seismic reconnaissance survey of the Mount Princeton area, Chaffee County, Colorado. MS thesis, Colorado School of Mines, T-1842.

CSM Field Camp report, unpublished results, Colorado School of Mines, dept. of Geophysics, 2009.

Dick, J. D. 1976. Geothermal Reservoir Temperatures in Chaffee County, Colorado. Thesis: Northeast Louisiana University, Monroe, Louisiana, pp. 1-171.

Dimick, N.J., 2007. The ability to predict ground water flow in a structurally faulted river valley with naturally occurring hot springs using multivariate geochemical analyses, MS Thesis, Colorado School of Mines, 93 pp., 2007.

Fairley, J.P., Heffner J., Hinds J.J., 2003. Geostatistical evaluation of permeability in an active fault zone. Geophysical Research Letters 30(18), 1962, doi:101029/2003GL018064.

Fairley, J.P., Hinds, J.J., 2004. Rapid transport pathways for geothermal fluids in an active

Great Basin fault zone. Geology 32, 825 – 828.

Faulds, J.E., and Varga, R.J., 1998. The role of accommodation zones and transfer zones in the regional segmentation of extensional terranes. Geol. Soc. Am. Special Paper 323, 45pp.

Garg S. K., Pritchett J. W., Wannamaker P. E., Combs J., 2007. Characterization of geothermal reservoirs with electrical surveys: Beowawe geothermal field. Geothermics 36, 487–517.

Gélis C., Revil, A., Cushing, M.E., Jougnot, D., Lemeille, F., et al. 2010. Potential of Electrical Resistivity Tomography to detect fault zones in limestone and argillaceous formations in the experimental site of Tournemire, France, in press in Pure and Applied Geophysics, doi: 10.1007/s00024-010-0097-x.

Gibbs A. D., 1984. Structural evolution of extensional basin margins. J. Geol. Soc. London 141, 609-620.

Hase, H., Ishido, T., Takakura, S., Hashimoto, T., Sato, K., Tanaka, Y., 2003. Zeta potential measurement of volcanic rocks from Aso caldera. Geophys. Res. Lett. 30, 2210, doi:10.1029/2003GL018694.

Heffner, J., Fairley, J.P., 2006. Using surface characteristics to infer the permeability structure of an active fault zone. Sedimentary Geology 184, 255 – 265.

Henderson, F., Olson, H., Berkman, F., Batzle, M., Revil, A., 2009. Future geothermal electrical production from Mount Princeton Hot Springs, Colorado. AAPG Search and Discovery Article, 2009 AAPG Annual Convention and Exhibition, Denver, Colorado, June 7-10, 2009.

Ishido, T., 1989. Self-potential generation by subsurface water flow through electrokinetic coupling, in Detection of Subsurface Flow Phenomena, Lecture Notes in Earth Sciences,Vol. 27, pp. 121–131, eds Merkler, G.-P., Militzer, H., Hötzl, H., Armbruster, H., Brauns, J., Springer-Verlag, Berlin.

Ishido, T., Pritchett, J.W., 1999. Numerical simulation of electrokinetic potentials associated with subsurface fluid flow. J. Geophys. Res. 104(B7), 15 247–15 259.

Ishido, T., 2004. Electrokinetic mechanism for 'W'-shaped self-potential profile on volcanoes. Geophys. Res. Lett. 31, L15616, doi:10.1029/2004GL020409.

Jardani A., Revil A., Bolève A., Dupont J.P., Barrash W., Malama B., 2007. Tomography of groundwater flow from self-potential (SP) data. Geophysical Research Letters 34, L24403, doi:10.1029/2007GL031907.

Jardani, A., Revil, A., Bolève, A., Dupont, J.P., 2008. 3D inversion of self-potential data used to constrain the pattern of ground water flow in geothermal fields. Journal of Geophysical Research 113, B09204, doi: 10.1029/2007JB005302.

Jardani, A., Revil, A., 2009. Stochastic joint inversion of temperature and self-potential data. Geophysical Journal International 179(1), 640-654, doi: 10.1111/j.1365-246X.2009.04295.x.

Jardani, A., Revil, A., Barrash, W., Crespy, A., Rizzo, E., Straface, S. Cardiff, M., Malama, B., Miller, C., and Johnson, T., 2009. Reconstruction of the water table from self potential data: A Bayesian approach. Ground Water 47(2), 213-227.

Legaz, A., A., Revil, P. Roux, J., Vandemeulebrouck, P. Gouédard, T., Hurst, and A. Bolève, 2009. Self-potential and passive seismic monitoring of hydrothermal activity: A case study at Iodine Pool, Waimangu geothermal valley, New Zealand. Journal of Volcanology and Geothermal Research 179(1-2), 11-18.

Leroy, P., Revil A., 2004. A triple layer model of the surface electrochemical properties of clay minerals. Journal of Colloid and Interface Science 270(2), 371-380.

Leroy, P., Revil A., 2009. Spectral induced polarization of clays and clay-rocks. Journal of Geophysical Research 114, B10202, doi:10.1029/2008JB006114.

Limbach, F.W., 1975. The geology of the Buena Vista area, Chaffee County, Colorado. MS

thesis, Colorado School of Mines, T-1692.

Loke, M.H., Barker, R.D., 1996. Practical techniques for 3D resistivity surveys and data inversion. Geophysical Prospecting 44, pp. 499–523.

McCalpin, J.P., Shannon, J.R., 2005. Geologic map of the Buena Vista West quadrangle, Chaffee County, Colorado, Technical Report, Colorado Geological Survey.

Malama, B., Revil A., Kulhman K.L., 2009a. A semi-analytical solution for trensient streaming potentials associated with confined aquifer pumping tests. Geophysical Journal International 176, 1007-1016, doi: 10.1111/j.1365-246X.2008.04014.x.

Malama, B., Kuhlman K.L., Revil A., 2009. Theory of transient streaming potentials associated with axial-symmetric flow in unconfined aquifers. Geophysical Journal International 179, 990–1003, doi: 10.1111/j.1365-246X.2009.04336.x.

Miller, M.G., 1999. Active breaching of a geometric segment boundary in the Sawatch Range normal fault, Colorado, USA. Journal of Structural Geology 21, 769-776.

Morgan, P., Sares, M., 2009. Strain partitioning in synthetic accommodation zones and selected geothermal systems in Colorado. Annual Meeting of the Geological Society of America, Portland Oregon, 18-21 October 2009.

Olson, H.J., Dellechaie F., 1976. The Mount Princeton geothermal area, Chaffee County, Colorado, Epis R.C., and Weimer, R.I., eds. Studies in Colorado Field Geology, Prof. Contr. Colorado School of Mines, n°8, Chap. 32, Nov., 552 p.

Onizawa, S. Matsushima, N., Ishido, T., Hase, H., Takakura, S., Nishi, Y., 2009. Self-potential distribution on active volcano controlled by three-dimensional resistivity structure in Izu-Oshima, Japan. Geophys. J. Int., 178(2), 1164-1181, doi: 10.1111/j.1365-246X.2009.04203.x.

Pearl, R. H. 1979. Colorado's Hydrothermal Resource Base – An Assessment. Colorado Geological Survey, Resource Series 6, 1-144.

Pearl, R. H. 1972. Geothermal Resources of Colorado. Colorado Geological Survey, Special Publication 2, pp. 1-54.

Perrier, F., Richon, P., Byrdina, S., France-Lanord, C., Rajaure, S., Koirala, B., Shrestha, P. L., Gautam, U.P., Tiwari, D.R., Revil, A., Bollinger, L., Contraires, S., Bureau, S., Sapkota, S.N., 2009. A direct evidence for high carbon dioxide and radon-222 discharge in Central Nepal. Earth and Planetary Research Letters 278, 198-207.

Poldini, E., 1938. Geophysical exploration by spontaneous polarization methods, Mining Mag. London, 59, 278-282.

Revil, A., Pezard, P.A., 1998. Streaming potential anomaly along faults in geothermal areas. Geophysical Research Letters 25(16), 3197-3200.

Revil, A., Cathles, L.M., Losh, S., Nunn, J.A., 1998. Electrical conductivity in shaly sands with geophysical applications. Journal of Geophysical Research 103(B10), 23,925-23,936.

Revil, A., Leroy P., 2001. Hydroelectric coupling in a clayey material. Geophysical Research Letters 28(8), 1643-1646.

Revil, A., Cathles L. M., 2002. Fluid transport by solitary waves along growing faults: a field example from the South Eugene Island Basin, Gulf of Mexico. Earth and Planetary Science Letters 202(2), 321-335 (erratum: Revil, A. Cathles L.M., Fluid transport by solitary waves along growing faults: a field example from the South Eugene Island Basin, Gulf of Mexico. Earth and Planetary Science Letters 204(1-2), 321-322, 2002).

Revil, A., Naudet, V., Nouzaret, J., Pessel, M., 2003. Principles of electrography applied to self-potential electrokinetic sources and hydrogeological applications. Water Resour. Res. 39(5), 1114, doi:10.1029/2001WR000916.

Revil, A., L. Cary, Q. Fan, A. Finizola, and F. Trolard, 2005. Self-potential signals associated with preferential ground water flow pathways in a buried paleo-channel. Geophysical Research Letters 32, L07401, doi:10.1029/2004GL022124.

Revil, A., Leroy, P., Titov, K., 2005. Characterization of transport properties of argillaceous sediments. Application to the Callovo-Oxfordian Argillite, Journal of Geophysical Research 110, B06202, doi: 10.1029/2004JB003442.

Revil A., Finizola, A., Piscitelli, A., Rizzo, E., Ricci, T., et al., 2008. Inner structure of La Fossa di Vulcano (Vulcano Island, southern Tyrrhenian Sea, Italy) revealed by high resolution electric resistivity tomography coupled with self-potential, temperature, and soil CO_2 diffuse degassing measurements. Journal of Geophysical Research 113, B07207, doi:10.1029/2007JB005394

Revil, A., A. Jardani, and K. Richards (2010), Non-intrusive estimate of the flow rate of thermal water along tectonic faults. Theory and application, in press in Geophysical Research Letters.

Scott, G.R., Van Alstine, R.E., Sharp, W.N., 1975. Geologic map of the Poncha Springs quadrangle, Chaffee County, Colorado. U.S. Geological Survey Miscellaneous Field Studies Map MF-658, scale 1:62,500.

Suski, B., Revil, A., Titov, K., Konosavsky, P., Dagès, C., Voltz, M., Huttel, O., 2006. Monitoring of an infiltration experiment using the self-potential method. Water Resources Research 42, W08418, doi:10.1029/2005WR004840.

Suski, S., Brocard, G., Authemayou, C., Muralles, B.C., Teyssier, C., Holliger, K., 2010. Localization and characterization of an active fault in an urbanized area in central Guatemala by means of geoelectrical imaging, Tectonophysics 480(1-4), 88-98.

Table

Table 1. Mean composition of the non-thermal water with standard deviation (from Dimick, 2007). Concentrations are in mg L^{-1}. Statistics determined using 23 samples.

Property	Mean and deviation
T (°C)	13±7
pH (-)	7.8±0.4
σ_f (10^{-2} S m^{-1}, 25°C)	1.86±0.40
K^+	1.4±0.5
Na^+	9.3±8.0
Ca^{2+}	23.7±8.9
Mg^{2+}	3.2±1.6
SiO_2(aq)	15.6±4.7
HCO_3^-	93.6±26.4
SO_4^{2-}	12.1±9.8
Cl^-	1.8±1.4
F^-	0.4±0.3

Table 2. Composition of the thermal water (from Dimick, 2007).

Property	Sample 4(1)	Sample 5(1)	Sample 6 (2)	Sample 7 (3)
T (°C)	54	54	82	67
pH (-)	8.6	7.9	8.5	-
σ_f (10^{-2} S m^{-1}, 25°C)	3.33	3.21	4.80	2.40
K^+	2.10	2.20	3.10	2.10
Na^+	58	57	94	61
Ca^{2+}	10	11	4.4	8.30
Mg^{2+}	0.20	0.90	0.10	0.30
SiO_2(aq)	58	56	68	53
HCO_3^-	67	75	71	68
SO_4^{2-}	69	64	100	60
Cl^-	5.3	5.3	10	4.9
F^-	8.3	10	14	10

(1) Mount Princeton Hot Springs (sampling: Oct. 1975 and Jan. 1976, respectively)

(2) Hortense Hot Springs (sampling Oct. 1975)

(3) Wright Hot Springs (sampling Aug. 1975)

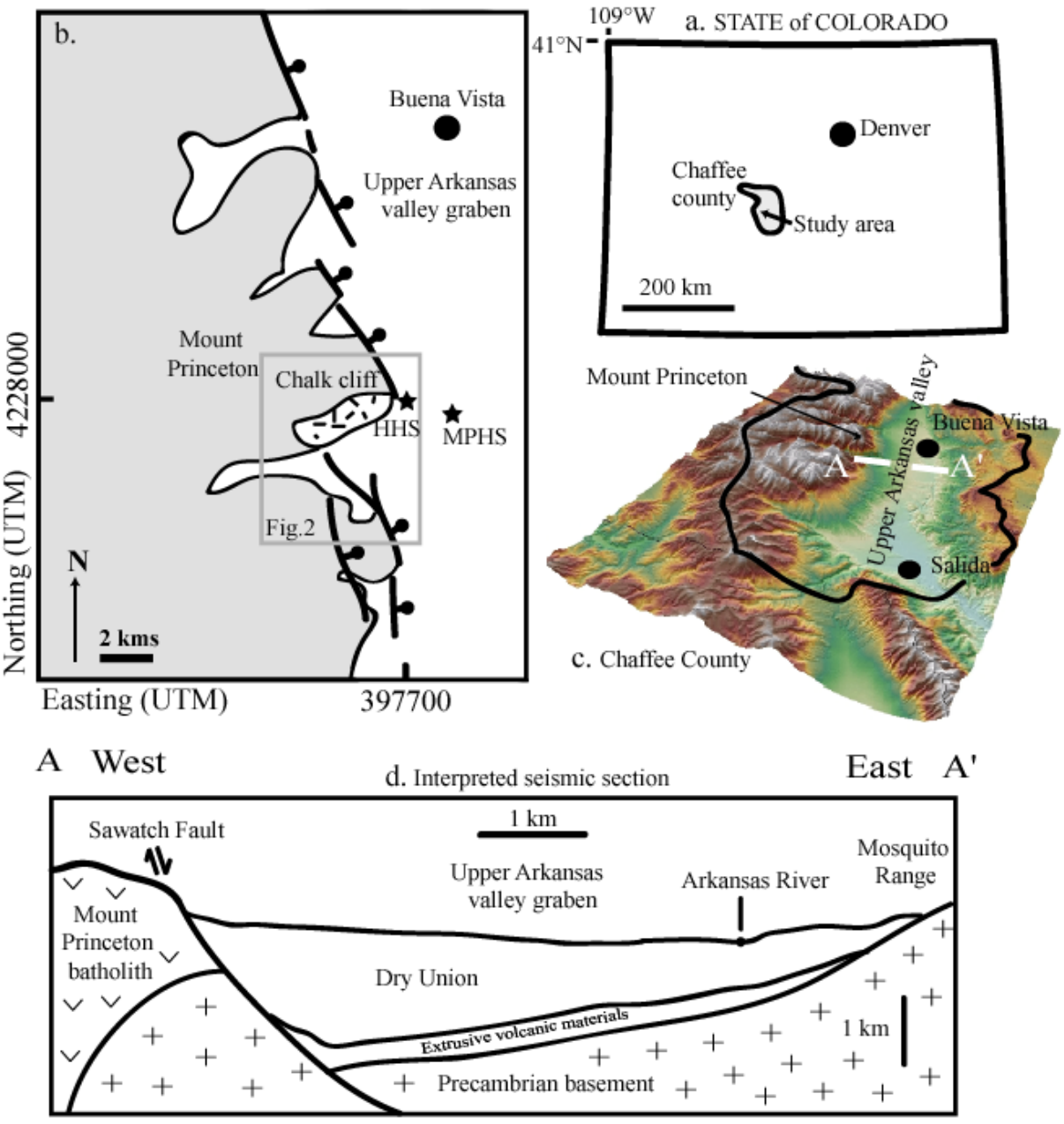

Figure 1. Localization of the study area. **a.** Sketch of the State of Colorado. **b.** Simplified geological sketch showing the position of the Sawatch Range fault along the Sawatch Range as it appears on the maps by Scott et al. (1975), Colman et al. (1985), and Miller (1999). The gray background indicates the bedrock (quartz monzonite of Mount Princeton batholith) while off-white indicates Quaternary materials. HHS and MPHS correspond to the Hortense Hot Springs and Mount Princeton Hot Springs, respectively. **c.** Map of Chaffee County. **d.** Simplified cross-section of the Upper Arkansas graben (CSM Field Camp report, 2009). UTM zone: 13 South.

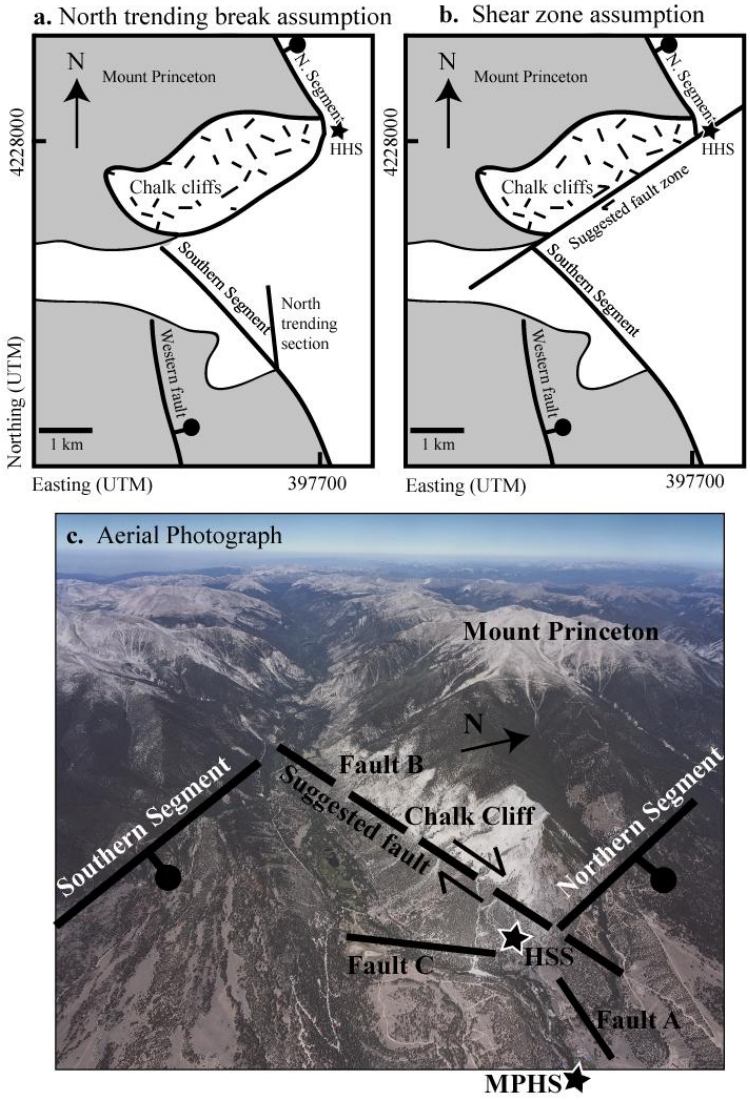

Figure 2. Simplified geological sketches (insert of Figure 1) showing the position of the Northern and southern segments of the Sawatch Range fault near Chalk Cliffs as it appears on the maps by Scott et al. (1975) and Colman et al. (1985). The gray background indicates the bedrock (quartz monzonite of Mount Princeton batholith), off-white indicates Quaternary materials. HHS corresponds to the Hortense Hot Springs. We have also indicated the position of the dextral strike slip fault zone (Fault B) inferred from the present study **a.** Breaching model proposed by Miller (1999). **b.** Dextral strike slip zone model proposed in the present paper and supported by the geoelectrical data. **c.** Aerial photograph of the investigated area (courtesy from Jeffrey A. Coe, USGS) and approximate position of the faults discussed in the main text (Faults A, B and C) including the dextral strike slip zone between the North and South segments of the range front fault. The photograph is showing Mount Princeton, which is part of the collegial peaks, and the Chalk Cliff. UTM zone is 13 South.

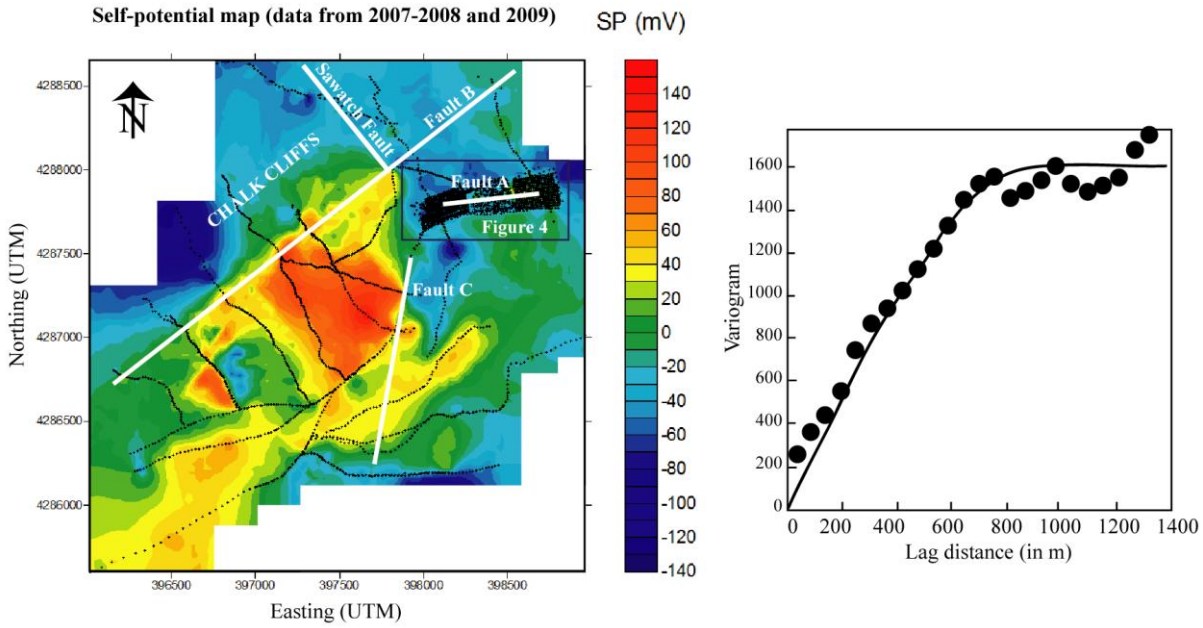

Figure 3. Self-potential (SP) map of the investigated area in mV. A total of 2700 measurements (the small black crosses) have been used to draw this self-potential map using kriging based on the fit of the semi-variogram. UTM zone is 13 South.

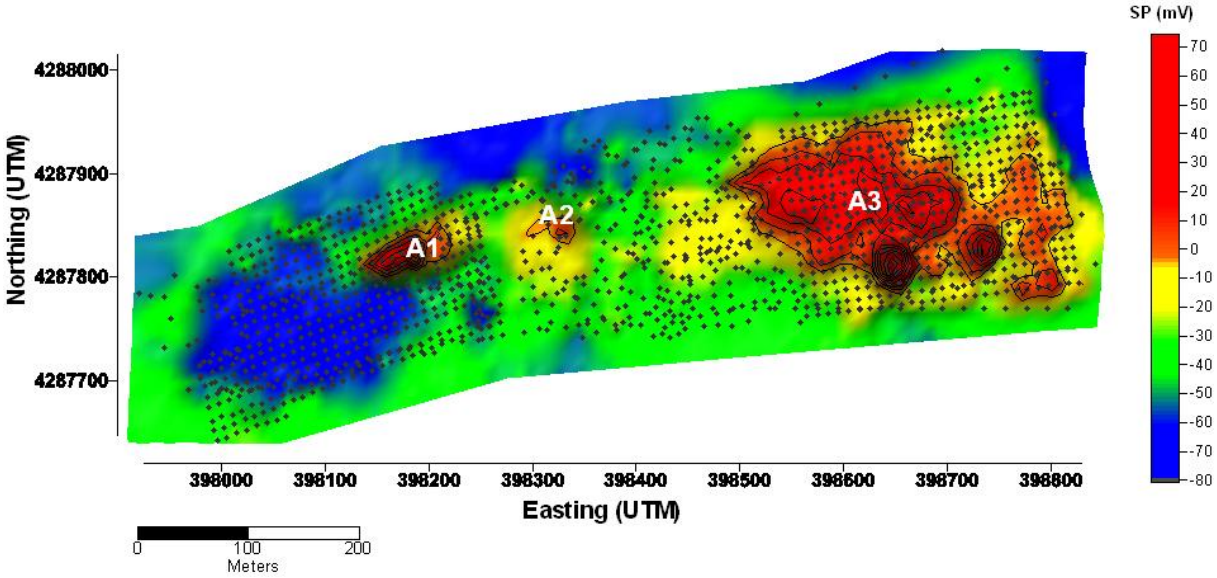

Figure 4. High resolution map of self-potential (SP) signals (in mV) (insert of Figure 3) at the tip of the Sawatch Range fault (see position in the insert of Figure 3) showing three nearly aligned positive self-potential anomalies (labeled A1, A2, and A3) along Fault A. These anomalies evidence areas of upflow of the thermal waters possibly along Fault A that may be plugged between A1 and A2 and between A2 and A3. A total of 1470 measurements have been used to draw this self-potential map using a kriging algorithm based on the fit of the semi-variogram. The self-potential stations are materialized by the black diamonds. The reference is the same as for Figure 3. The temperature of the ground water sampled downstream the anomaly A3 is 60°C. UTM zone is 13 South.

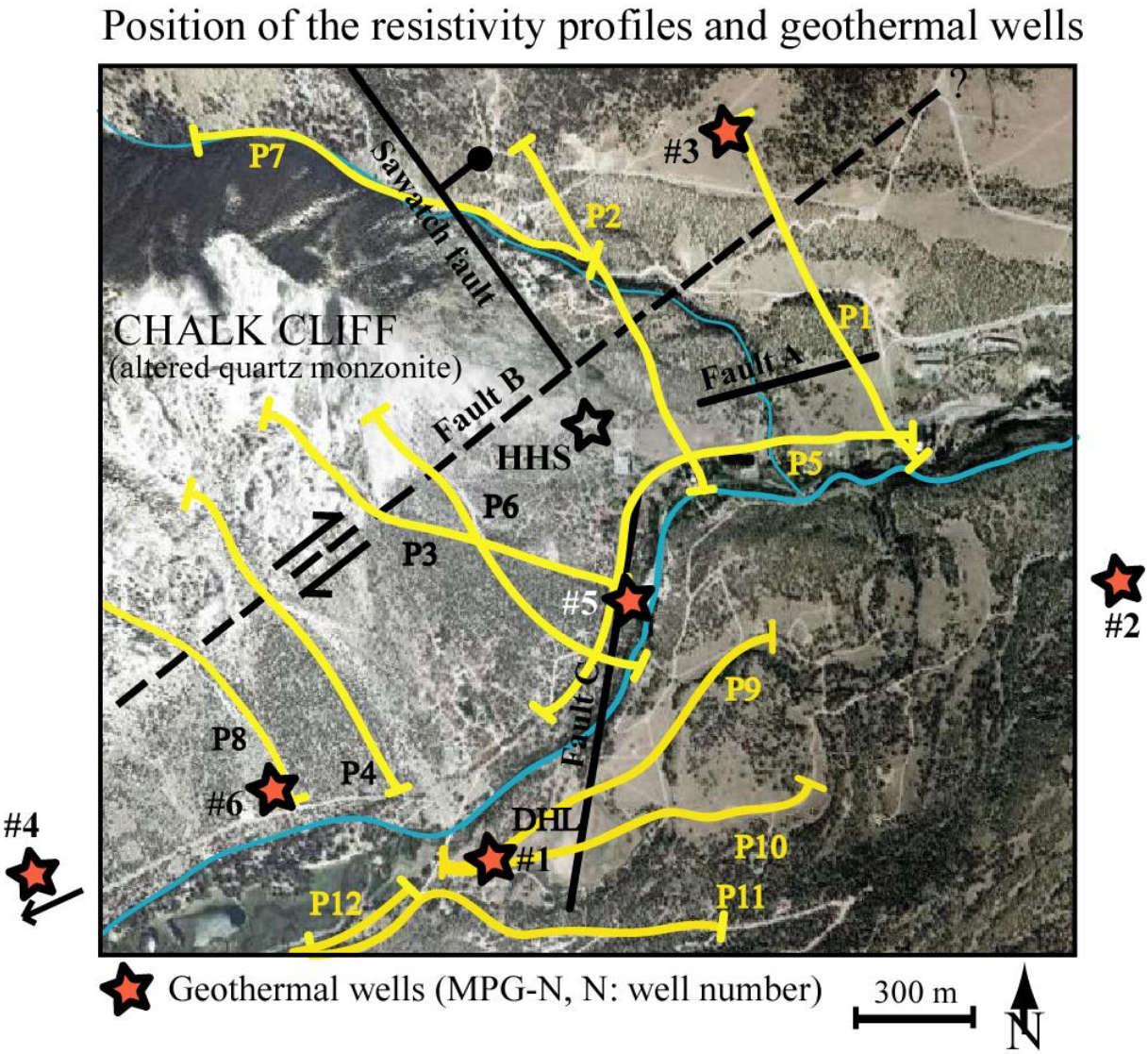

Figure 5. Map of the investigated area showing the position of the resistivity profiles and the position of the three main faults (Faults A, B, and C in our nomenclature) discussed in the text plus the Sawatch normal fault bordering the half-graben of the Upper Arkansas valley. DHL: Dead Horse Lake

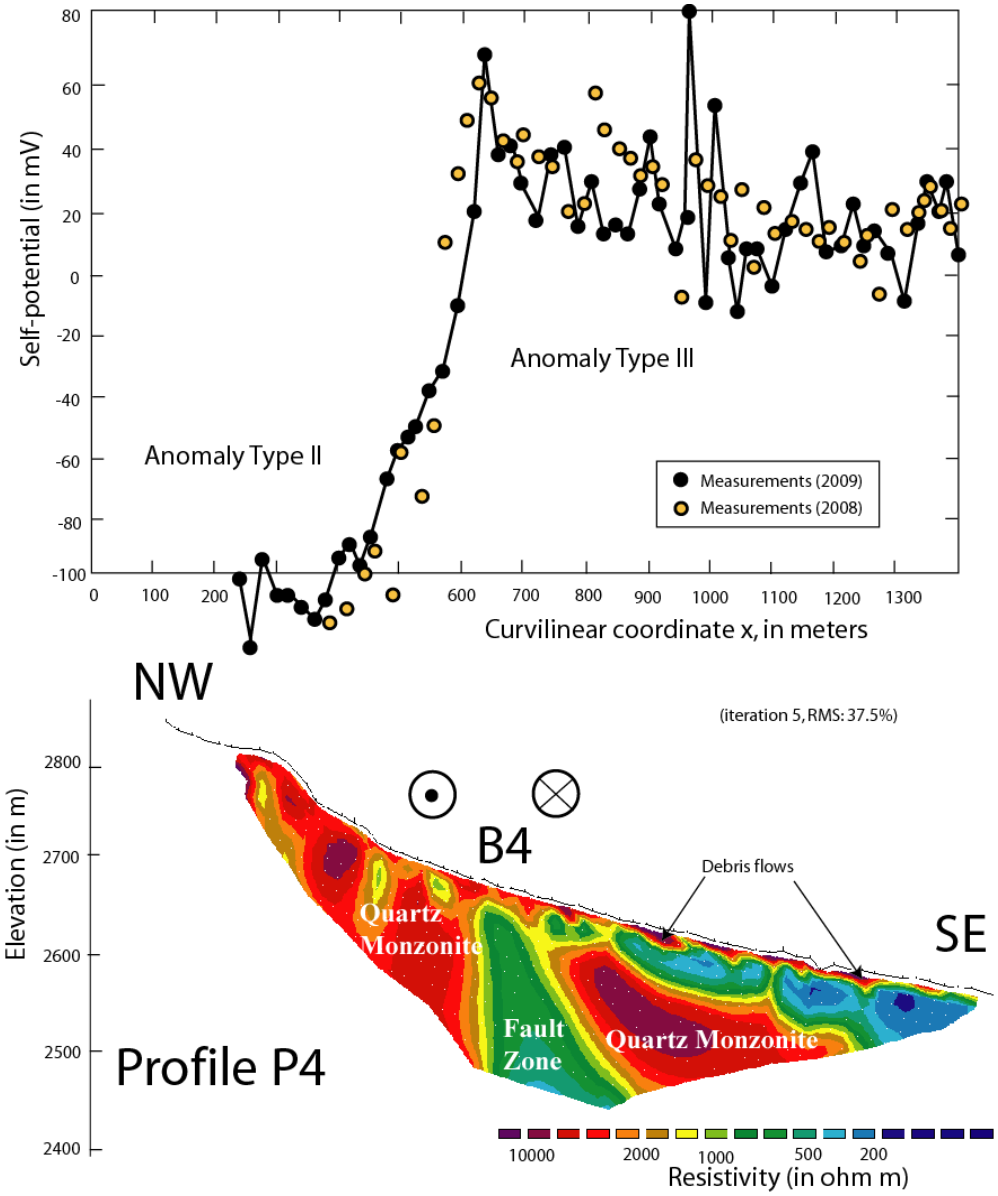

Figure 6. Resistivity tomogram (RMS Error 38%) and self-potential data along profile P4 (vertical exaggeration factor: 1.3). The conductive body B4 represents the position of the dextral strike slip zone. The fault is associated by a drop of 160 mV in the self-potential signals and resistivity values ranging from 300 to 500 ohm m, ten times lower than the resistivity of the unaltered quartz monzonite (2,000-10,000 ohm m). It seems that this portion of the dextral strike slip zone (Fault B) does not behave as a conduit as evidenced by the higher resistivity of the fault zone and the very high resistivity of the surrounding rocks indicating no alteration. The arrows show the displacement of the fault. The self-potential reference for this profile is arbitrary.

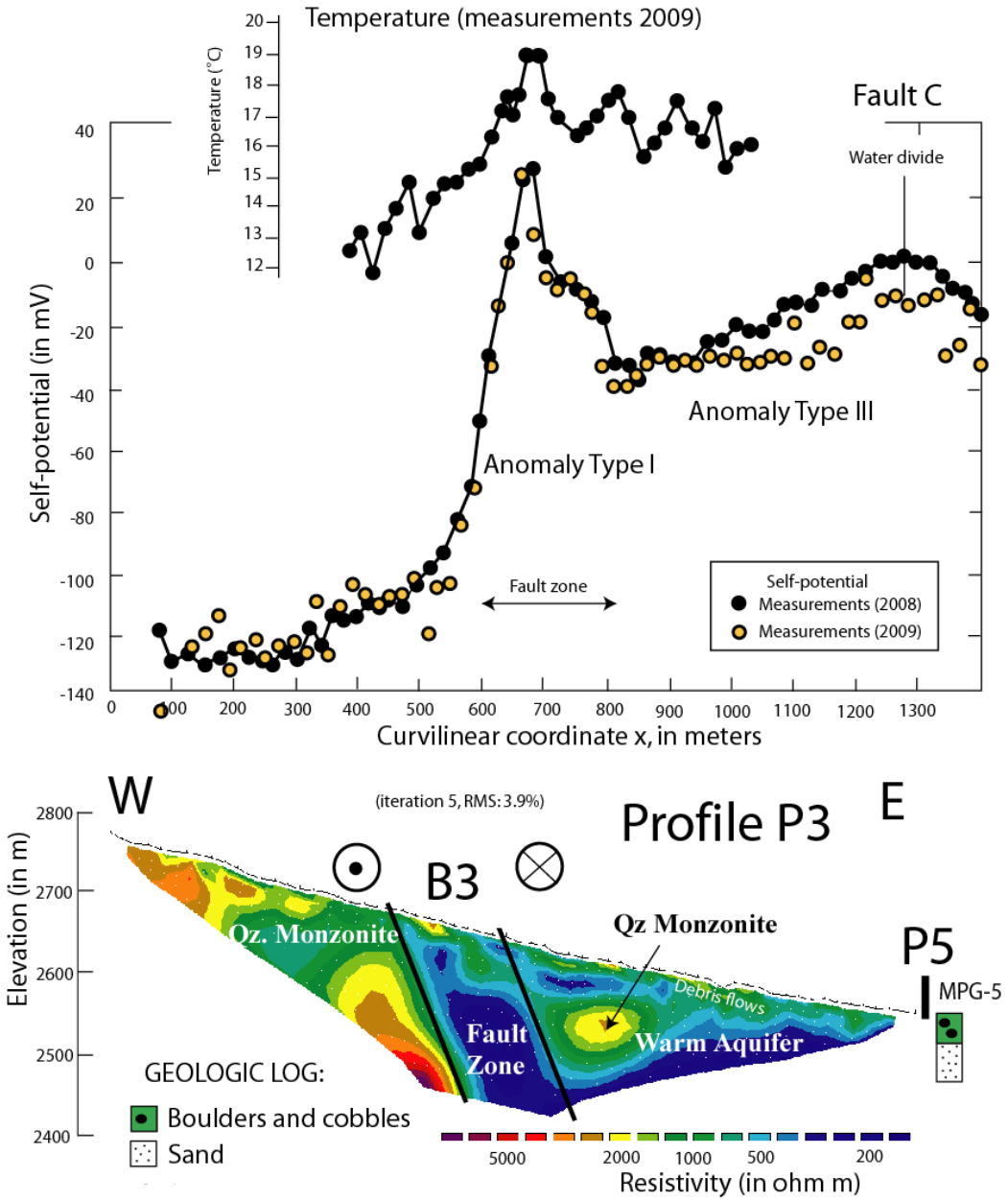

Figure 7. Resistivity tomogram (RMS Error 4%) and self-potential data along profile P3 (vertical exaggeration factor: 1.3). The conductive body B3 is associated with the dextral strike slip zone. The upflow in the dextral strike slip fault zone (Fault B) is associated by a self-potential anomaly of 150 mV in the self-potential signals, low resistivity values (in the range 100-300 ohm m), and an increase of the temperature at a depth of 30 cm. The positive self-potential anomaly evidences the up-flow of the hydrothermal fluids in this portion of the fault zone. Note the consistency of the self-potential measurements over a year of time interval. The arrows represent the displacement of the fault. The self-potential reference for this profile is arbitrary.

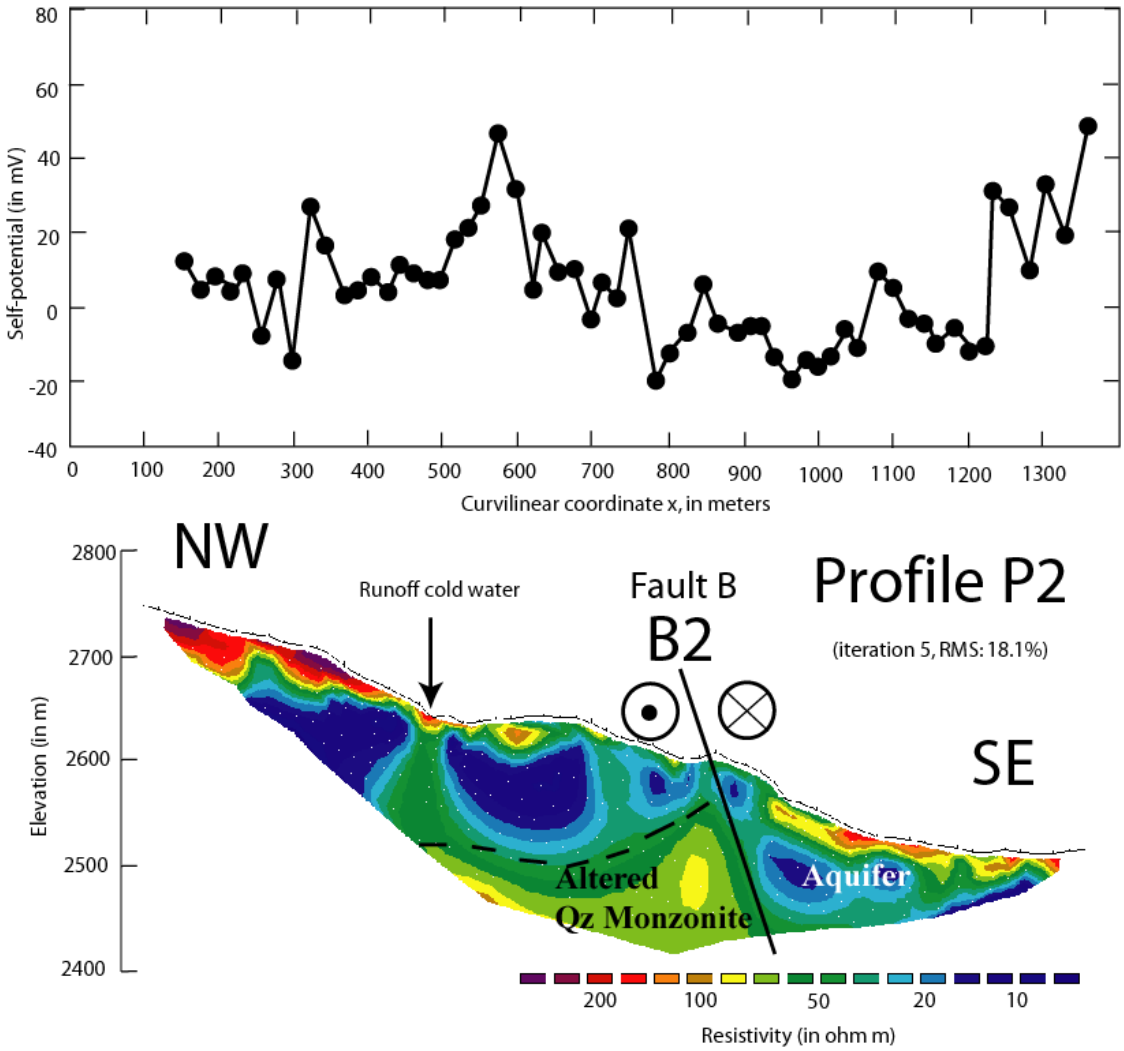

Figure 8. a. Resistivity tomogram (RMS Error 18%) and self-potential data along profile P2 at the intersection between the dextral strike slip zone and the Sawatch fault (vertical exaggeration factor: 1.3). The plane B2 is in the direction of the dextral strike slip fault zone evidenced in profiles P3 and P4. Note the scale of the resistivity values showing very low conductivities all over this profile by comparison with Profiles 3 and 4. The runoff of cold water at the surface is probably responsible for a mix of cold and thermal waters in the upper part of the shallow aquifer. The arrows represent the displacement of the fault.

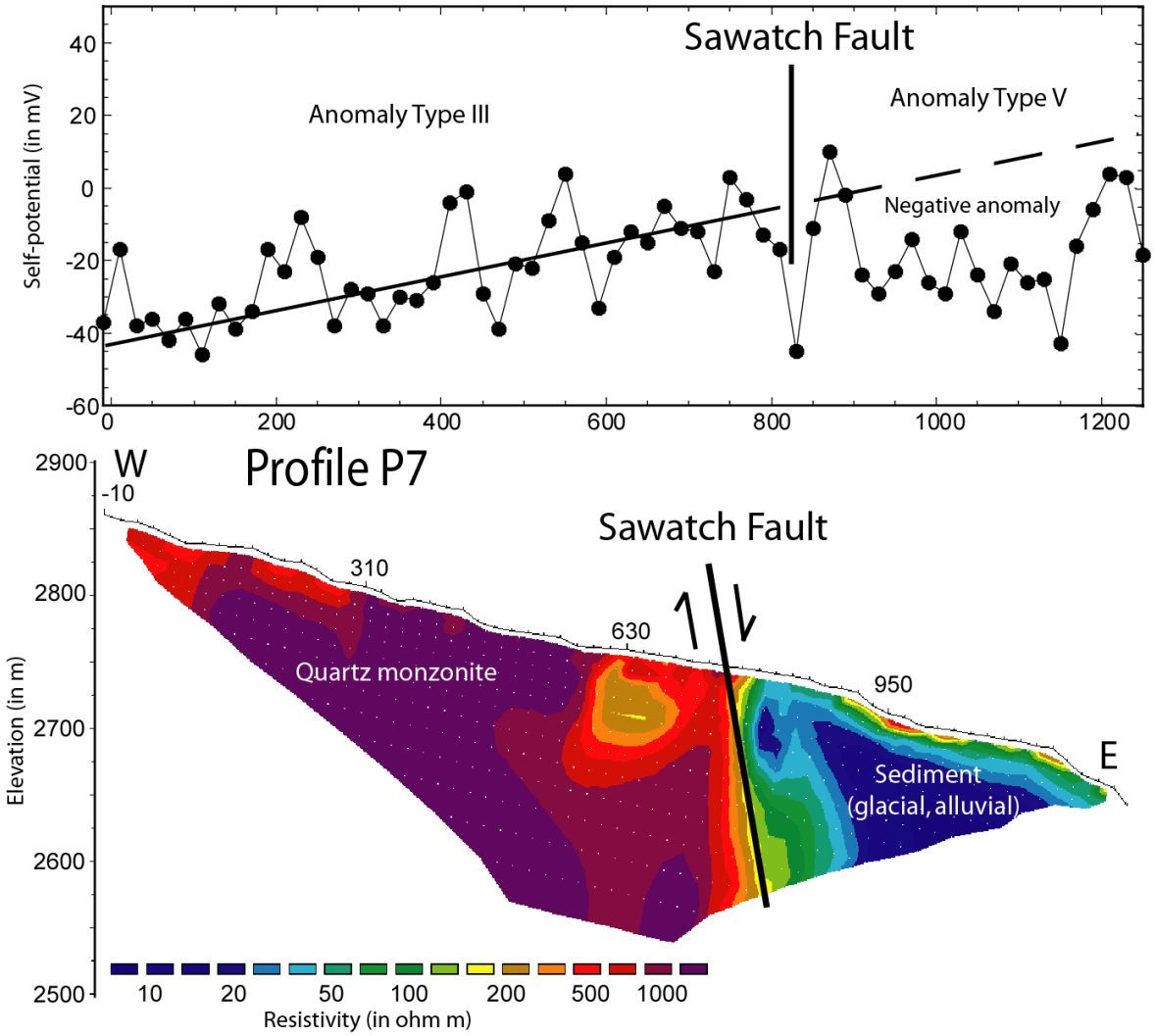

Figure 9. Resistivity tomogram (iteration 2, RMS Error 9%) and self-potential data along profile P7 crossing the Sawatch fault (vertical exaggeration factor: 1.6). The position of the fault agrees with the position of a fault plane inferred from surface observations. The self-potential reference for this profile is arbitrary. The self-potential profile shows a classical positive trend going downslope (topographic effect) in the upper part of the section that is associated with the downward flow of water in a very shallow aquifer (type III) associated with the runoff of a small river. On the Eastern part of the fault, the self-potential shows a negative anomaly with respect to the previous trend. This indicates a change in the ground water flow direction (Type V) or possibly infiltration of the ground water from the river in a shallow aquifer.

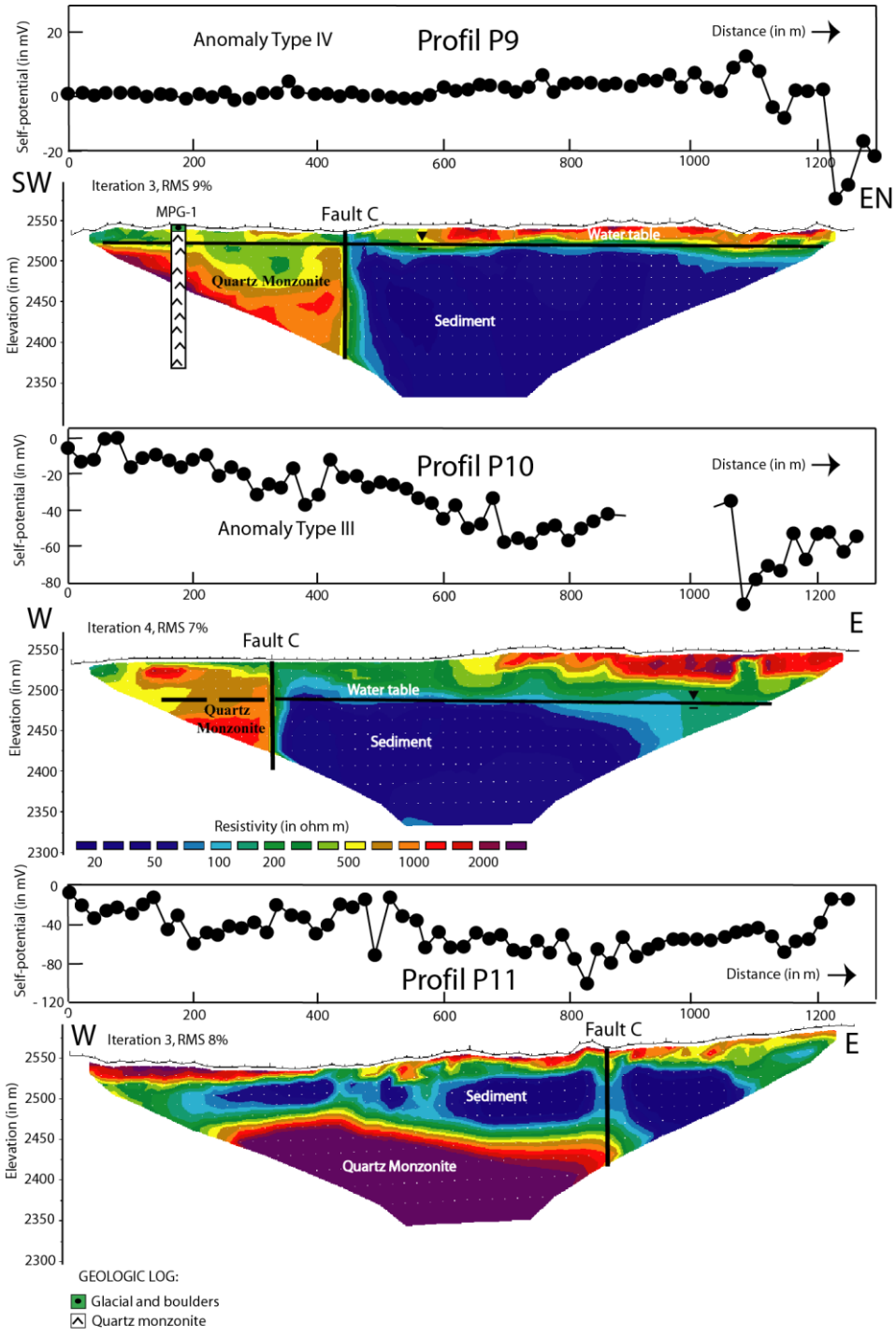
Anomaly Type IV
Profil P9
Distance (in m)
Self-potential (in mV)
SW
EN
Iteration 3, RMS 9%
MPG-1
Fault C
Water table
Quartz Monzonite
Sediment
Elevation (in m)
Profil P10
Anomaly Type III
W
E
Iteration 4, RMS 7%
Resistivity (in ohm m)
Profil P11
Iteration 3, RMS 8%
GEOLOGIC LOG:
Glacial and boulders
Quartz monzonite

Figure 10.

Figure 10. Resistivity tomograms P9, P10, and P11 (with the same resistivity scale) and self-potential data along these profiles. The low resistivity area (10-60 ohm m) corresponds to a shallow sedimentary aquifer. This aquifer is made of boulders, cobbles, aggregates, and sands. The resistive body on the west side of the profiles corresponds to the altered quartz monzonite. The boundary between the monzonite and the sediment corresponds to the Fault C. The self-potential reference for this profile is taken at $x = 0$.

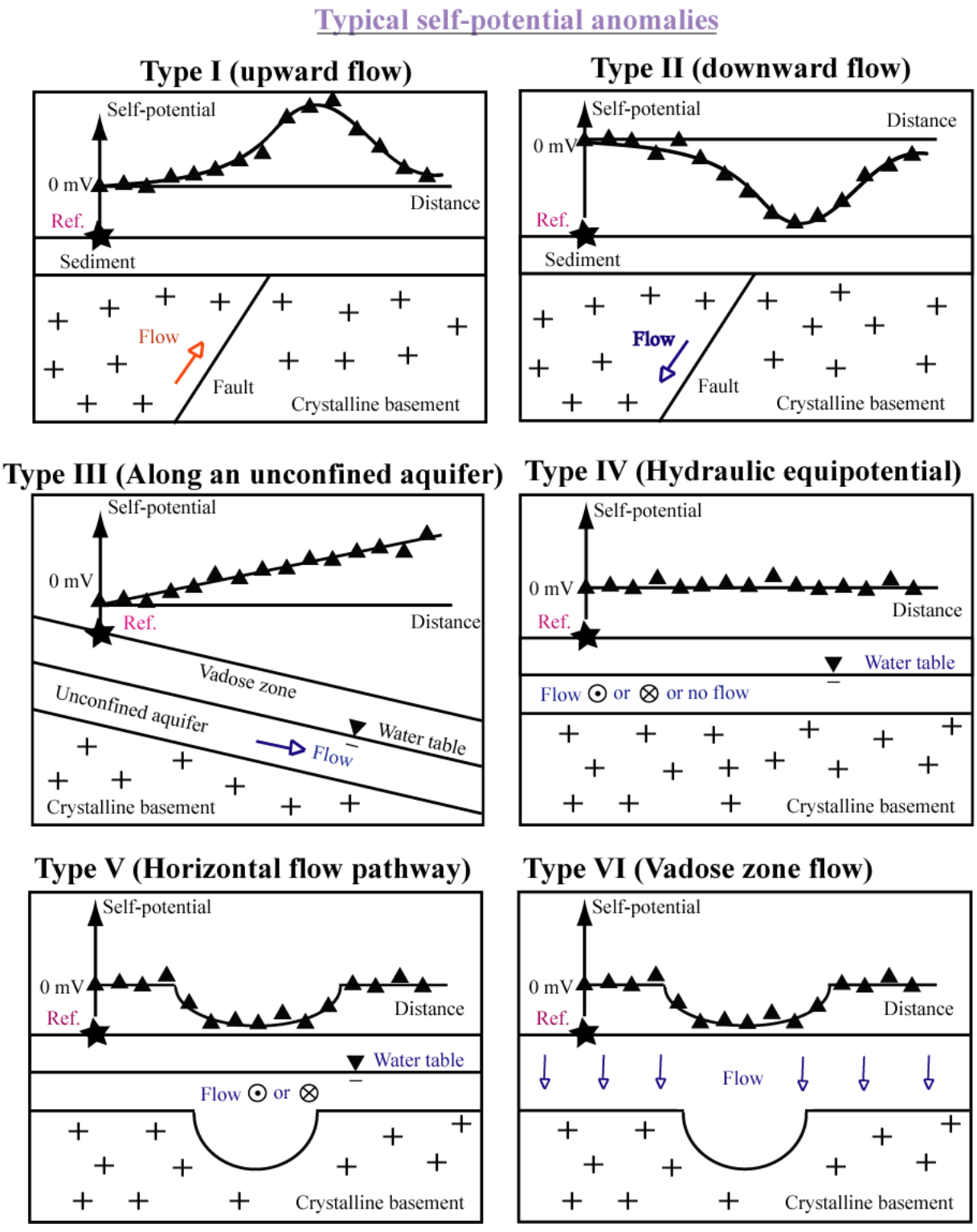

Figure 11. Typical self-potential anomalies and their potential hydrogeological meaning. The filled-triangles represent noisy self-potential measurements measured at the ground surface and "Ref" represents the reference electrode (zero potential) used for the profiles.

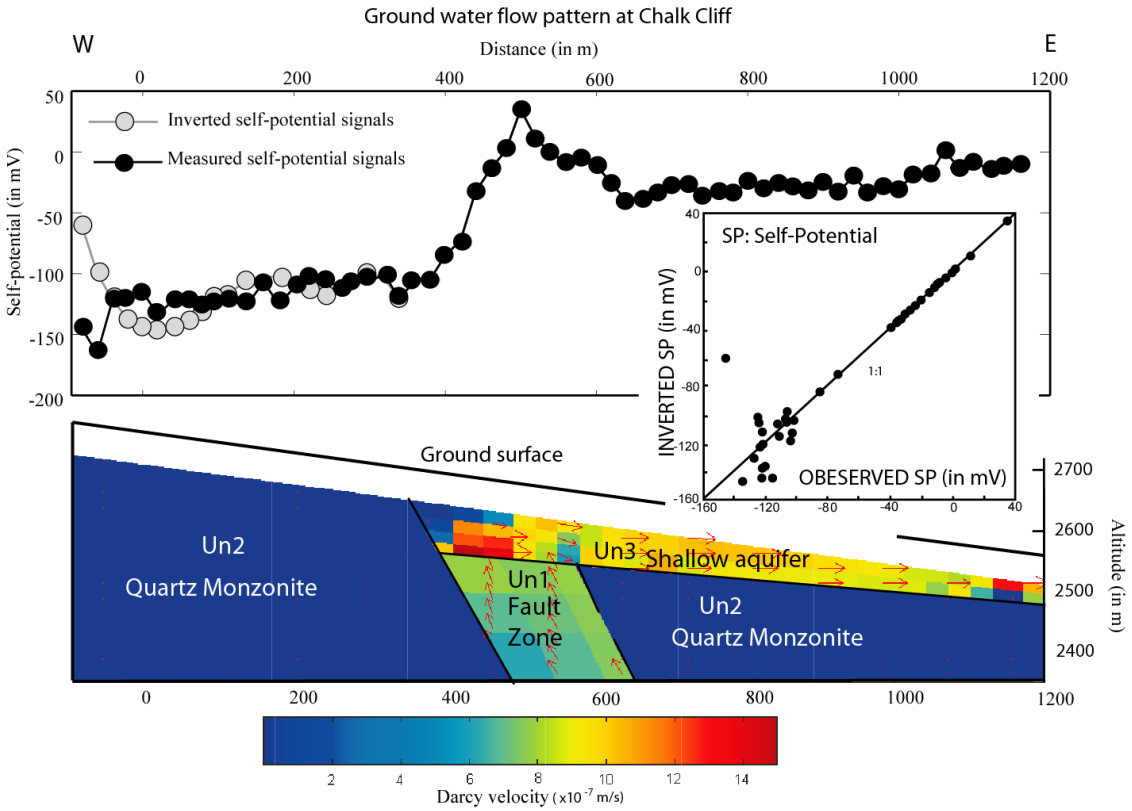

Figure 12. Ground water flow pattern as constrained by DC-resistivity and self-potential data along profile P3 (data from 2008, the beginning of the profile has been omitted). The unit U1 corresponds to the dextral strike slip zone, the unit Un2 to the quartz monzonite basement, and the unit Un3 to the shallow aquifer. The boundary conditions are (i) impervious boundaries except at the base of the dextral strike slip fault and at the outflow of the aquifer and (ii) insulating boundaries. In this model, we ignore the possibility of a mix between the thermal water and some cold water that would come from the upper section of the Chalk-cliffs. This may explained the discrepancy between the model and the data occurs at the top of the profile. The arrows and the colors represent the direction and the amplitude of the Darcy velocity, respectively. Insert: Comparison between the measured self-potential data and those resulting from the optimized ground water flow model (RMS=1.2%). The water table is ~at a depth of 40 m below the ground surface at the bottom of the profile as shown by MPG-5 (Figure 5).

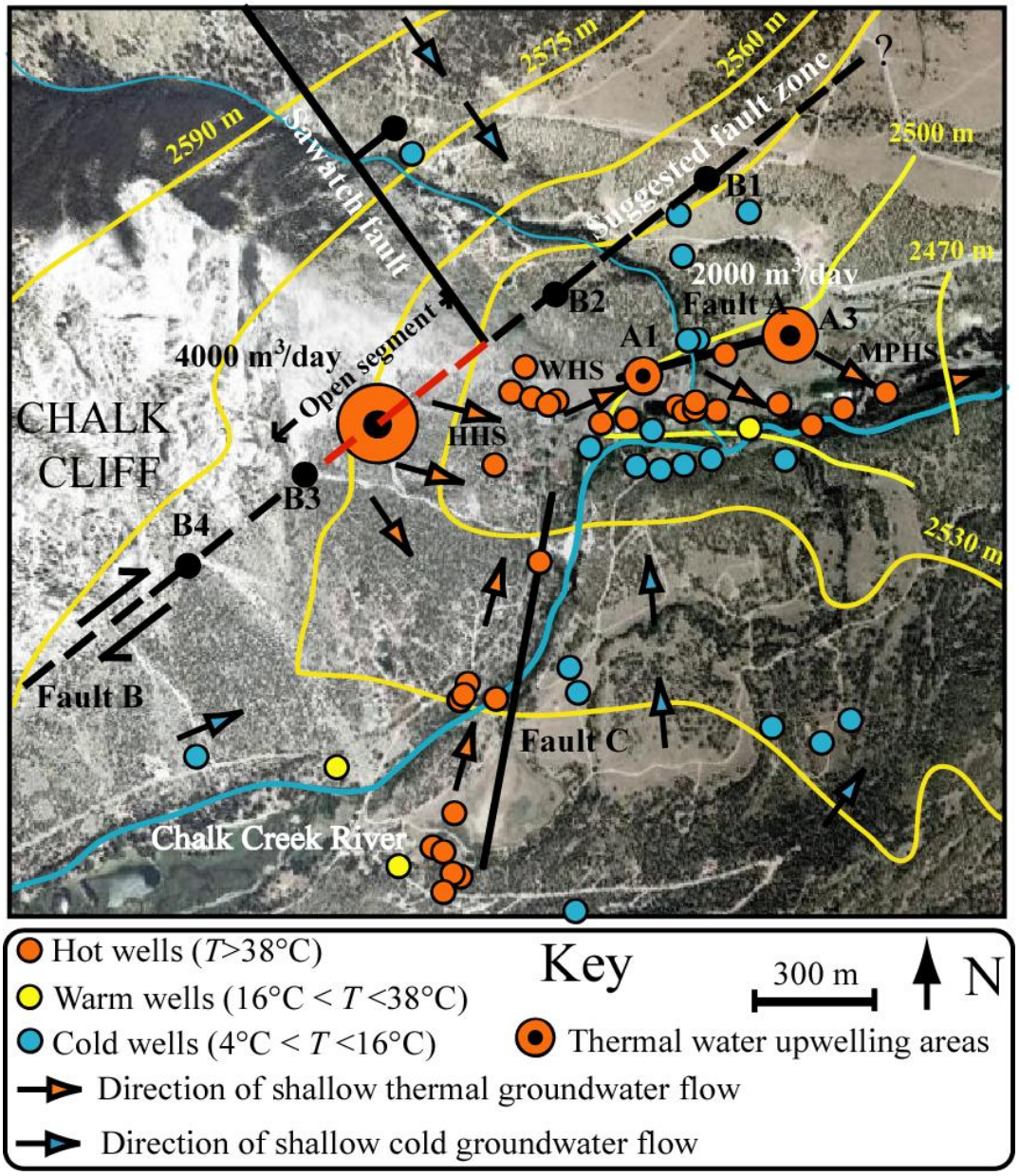

Figure 13. Piezometric map and shallow ground water flow model. The map shows the position of the cold, warm, and hot (mostly domestic) wells (spring temperatures) and the position of the faults. B1 to B4 represents the position of the electrical conductivity anomalies associated with the dextral strike slip fault zone. A1 and A3 are positive self-potential anomalies shown in Figure 4 that materialized an open fracture. The position of the dextral strike slip zone (Fault B) is determined from the resistivity profiles. HHS, MPHS, and WHS correspond to Hortense Hot Springs, Mount Princeton Hot Springs, and Wright Hot Springs, respectively (see composition of the thermal waters in Table 2), and MPG-5 is a geothermal drill-hole. The piezometric surface is determined by ordinary kriging including wells outside the area shown on the map to avoid edge effects.

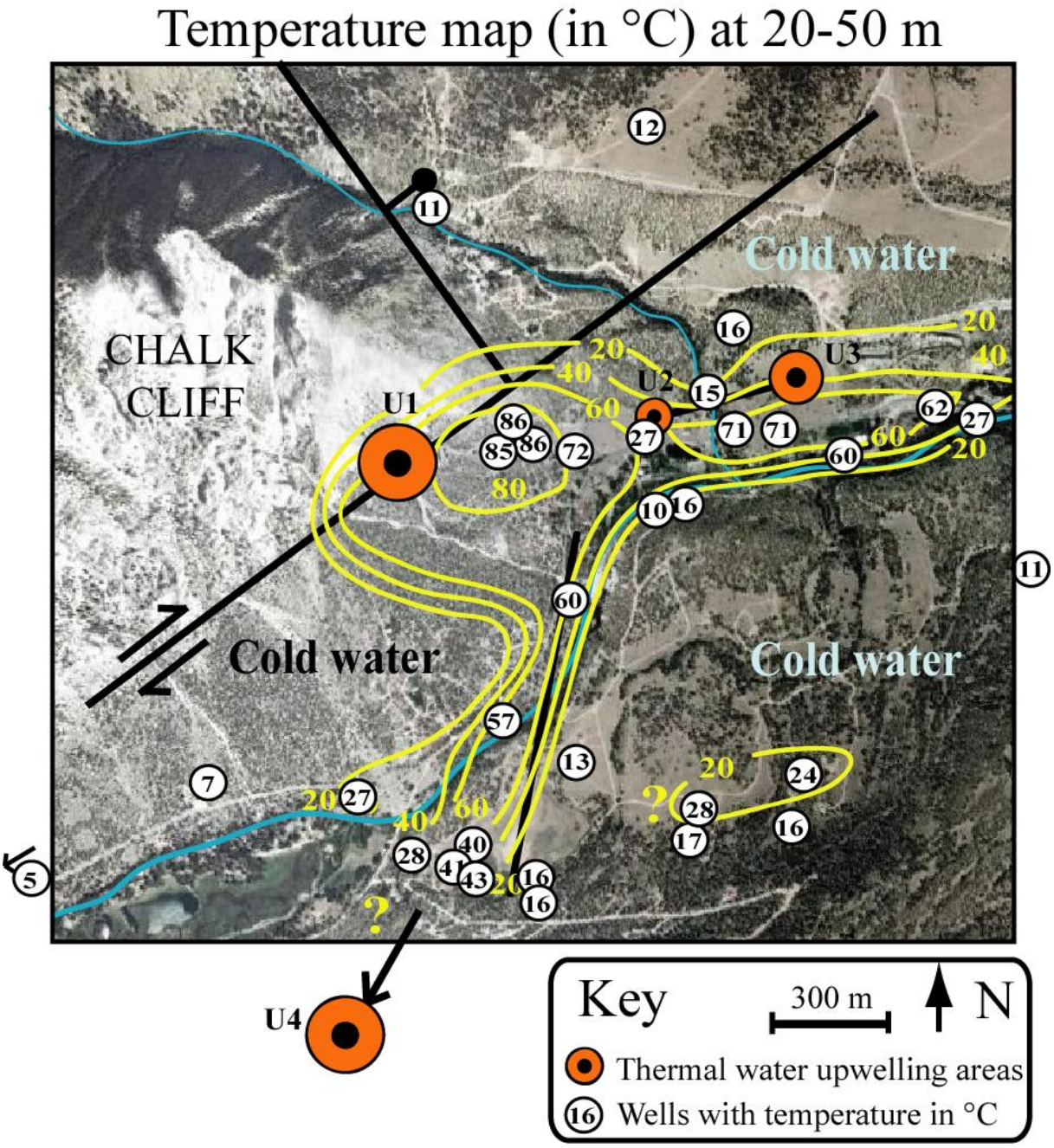

Figure 14. Temperature map in the depth range 20-50 m below the ground surface. The distribution of temperature implies the existence of a fourth area of thermal water upwelling area named U4. This area may be located further south west of the investigated area. This area is possibly located at the tip of one of the southern segments of the Sawatch Fault (see Figure 2).